Chapter 12

Layered Models

ABSTRACT

The assumption of density conservation by fluid parcels is advantageously used to change the vertical coordinate from depth to density. The new equations offer a clear discussion of potential-vorticity dynamics and lend themselves to discretization in the vertical. The result is a layered model. Splitting stratification in a series of layers may be interpreted as a vertical discretization in which the vertical grid is a material surface of the flow. This naturally leads to the presentation of Lagrangian approaches. *Note*: To avoid problems of terminology, we restrict ourselves here to the ocean. The case of the atmosphere follows with the replacement of depth by height and density by potential density.

12.1 FROM DEPTH TO DENSITY

Since a stable stratification requires a monotonic increase of density downward, density can be taken as a surrogate for depth and used as the vertical coordinate. If density is conserved by individual fluid parcels, as it is approximately the case for most geophysical flows, considerable mathematical simplification follows, and the new equations present a definite advantage in a number of situations. It is thus worth expounding on this change of variables at some length.

In the original Cartesian system of coordinates, z is an independent variable, and density $\rho(x, y, z, t)$ is a dependent variable, giving the water density at location (x, y), time t, and depth z. In the transformed coordinate system (x, y, ρ, t), density becomes an independent variable, and $z(x, y, \rho, t)$ has become the dependent variable giving the depth at which density ρ is found at location (x, y) and at time t. A surface along which density is constant is called an *isopycnal surface* or *isopycnic* for short.

Introduction to Geophysical Fluid Dynamics, Volume 101, ISSN 0074-6142, DOI: 10.1016/B978-0-12-088759-0.00012-2

From a differentiation of the expression $a = a(x, y, \rho(x, y, z, t), t)$, where a is any function, the rules for the change of are as follows:

$$\begin{aligned}
\frac{\partial}{\partial x} &\longrightarrow \left.\frac{\partial a}{\partial x}\right|_z = \left.\frac{\partial a}{\partial x}\right|_\rho + \frac{\partial a}{\partial \rho}\left.\frac{\partial \rho}{\partial x}\right|_z \\
\frac{\partial}{\partial y} &\longrightarrow \left.\frac{\partial a}{\partial y}\right|_z = \left.\frac{\partial a}{\partial y}\right|_\rho + \frac{\partial a}{\partial \rho}\left.\frac{\partial \rho}{\partial y}\right|_z \\
\frac{\partial}{\partial z} &\longrightarrow \frac{\partial a}{\partial z} = \frac{\partial a}{\partial \rho}\frac{\partial \rho}{\partial z} \\
\frac{\partial}{\partial t} &\longrightarrow \left.\frac{\partial a}{\partial t}\right|_z = \left.\frac{\partial a}{\partial t}\right|_\rho + \frac{\partial a}{\partial \rho}\left.\frac{\partial \rho}{\partial t}\right|_z .
\end{aligned}$$

Then, application to $a = z$ gives $0 = z_x + z_\rho \rho_x$, $1 = z_\rho \rho_z$, etc. (where a subscript indicates a derivative). This provides the rule to change the derivative of ρ at z constant to that of z at ρ constant. For a other than z, we can write

$$\left.\frac{\partial a}{\partial x}\right|_z = \left.\frac{\partial a}{\partial x}\right|_\rho - \frac{z_x}{z_\rho}\frac{\partial a}{\partial \rho}, \tag{12.1}$$

with similar expressions where x is replaced by y or t, and

$$\frac{\partial a}{\partial z} = \frac{1}{z_\rho}\frac{\partial a}{\partial \rho}. \tag{12.2}$$

Here, subscripts denote derivatives. Fig. 12.1 depicts a geometrical interpretation of rule (12.1).

The hydrostatic Eq. (4.19) readily becomes

$$\frac{\partial p}{\partial \rho} = -\rho g \frac{\partial z}{\partial \rho} \tag{12.3}$$

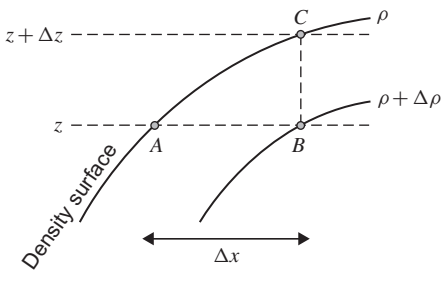

FIGURE 12.1 Geometrical interpretation of Eq. (12.1). The x-derivatives of any function a at constant depth z and at constant density ρ are $[a(B) - a(A)]/\Delta x$ and $[a(C) - a(A)]/\Delta x$, respectively. The difference between the two, $[a(C) - a(B)]/\Delta x$, represents the vertical derivative of a, $[a(C) - a(B)]/\Delta z$, times the slope of the density surface, $\Delta z/\Delta x$. Finally, the vertical derivative can be split as the ratio of the ρ-derivative of a, $[a(C) - a(B)]/\Delta\rho$, by $\Delta z/\Delta\rho$.

and leads to the following horizontal pressure gradient:

$$\left.\frac{\partial p}{\partial x}\right|_z = \left.\frac{\partial p}{\partial x}\right|_\rho - \frac{z_x}{z_\rho}\frac{\partial p}{\partial \rho} = \left.\frac{\partial p}{\partial x}\right|_\rho + \rho g \frac{\partial z}{\partial x} = \left.\frac{\partial P}{\partial x}\right|_\rho .$$

Similarly, $\partial p/\partial y$ at constant z becomes $\partial P/\partial y$ at constant ρ. The new function P, which plays the role of pressure in the density-coordinate system, is defined as

$$P = p + \rho g z \tag{12.4}$$

and is called the *Montgomery potential*.[1] Later on, when there is no ambiguity, this potential may loosely be called pressure. With P replacing pressure, the hydrostatic balance, (12.3), now takes a more compact form:

$$\frac{\partial P}{\partial \rho} = gz, \tag{12.5}$$

further indicating that P is the natural substitute for pressure when density is the vertical coordinate.

Beyond this point, all derivatives with respect to x, y, and time are meant to be taken at constant density, and the subscript ρ is no longer necessary.

With the use of Eqs. (12.1)–(12.3) and the obvious relation $\partial\rho/\partial x|_\rho = 0$, the density-conservation equation, (4.21e) in the absence of diffusion, can be solved for the vertical velocity

$$w = \frac{\partial z}{\partial t} + u\frac{\partial z}{\partial x} + v\frac{\partial z}{\partial y}. \tag{12.6}$$

This last equation simply tells that the vertical velocity is that necessary for the particle to remain at all times on the same density surface in analogy with surface fluid particles having to remain on the surface [see Eq. (7.12)]. Armed with expression (12.6), we can now eliminate the vertical velocity throughout the set of governing equations. First, the material derivative (3.3) assumes a simplified, two-dimensional-like form

$$\frac{\mathrm{d}}{\mathrm{d}t} = \frac{\partial}{\partial t} + u\frac{\partial}{\partial x} + v\frac{\partial}{\partial y}, \tag{12.7}$$

where the derivatives are now taken at constant ρ. The absence of an advective term in the third spatial direction results from the absence of motion across density surfaces.

[1] In honor of Raymond B. Montgomery who first introduced it in 1937. See his biography at the end of this chapter.

In the absence of friction and in the presence of rotation, the horizontal-momentum equations (4.21a) and (4.21b) become

$$\frac{\mathrm{d}u}{\mathrm{d}t} - fv = -\frac{1}{\rho_0}\frac{\partial P}{\partial x} \tag{12.8a}$$

$$\frac{\mathrm{d}v}{\mathrm{d}t} + fu = -\frac{1}{\rho_0}\frac{\partial P}{\partial y}. \tag{12.8b}$$

We note that they are almost identical to their original versions. The differences are nonetheless important: The material derivative is now along density surfaces and expressed by Eq. (12.7), the pressure p has been replaced by the Montgomery potential P defined in Eq. (12.4), and all temporal and horizontal derivatives are taken at constant density. Note, however, that the components u and v are still the true horizontal velocity components and are not measured along sloping density surfaces. This property is important for the proper application of lateral boundary conditions.

To complete the set of equations, it remains to transform the continuity equation (4.21d) according to rules (12.1) and (12.2). Further elimination of the vertical velocity by using Eq. (12.6) leads to

$$\frac{\partial h}{\partial t} + \frac{\partial}{\partial x}(hu) + \frac{\partial}{\partial y}(hv) = 0, \tag{12.9}$$

where the quantity h introduced for convenience is proportional to $\partial z/\partial\rho$, the derivative of depth with respect to density. For practicality, we want h to have the dimension of height, and so we introduce an arbitrary but constant density difference, $\Delta\rho$, and define

$$h = -\Delta\rho\frac{\partial z}{\partial\rho}. \tag{12.10}$$

In this manner, h can be interpreted as the thickness of a fluid layer between the density ρ and $\rho + \Delta\rho$. At this point, the value of $\Delta\rho$ is arbitrary, but later, in the development of layered models, it will naturally be chosen as the density difference between adjacent layers.

The transformation of coordinates is now complete. The new set of governing equations consists of the two horizontal-momentum equations (12.8a) and (12.8b), the hydrostatic balance (12.5), the continuity equation (12.9), and the relation (12.10). It thus forms a closed 5-by-5 system for the dependent variables, u, v, P, z, and h. Once the solution is known, the pressure p and the vertical velocity w can be recovered from Eqs. (12.4) and (12.6).

The governing equations are accompanied by the relevant boundary and initial conditions of Section 4.6. We only have to evaluate the derivatives of the Cartesian coordinates according to Eqs. (12.1) and (12.2) in order to impose the auxiliary conditions in the new coordinate system. The fluxes of heat and mass, leading to buoyancy changes, are not easily incorporated because of the

interplay with density, the new coordinate. Since processes that do not conserve density are neglected in most applications of isopycnal models, we will not investigate this point here but refer to Dewar (2001) for further details on the representation of mixed-layer dynamics in isopycnal models.

Since the aforementioned work of Montgomery (1937), the substitution of density as the vertical variable has been implemented in a number of applications, especially by Robinson (1965) in a study of inertial currents, by Hodnett (1978) and Huang (1989) in studies of the permanent oceanic thermocline, and by Sutyrin (1989) in a study of isolated eddies. A review in the meteorological context is provided by Hoskins, McIntyre and Robertson (1985).

12.2 LAYERED MODELS

A *layered model* is an idealization by which a stratified fluid flow is represented as a finite number of moving layers, stacked one upon another and each having a uniform density. Its evolution is governed by a discretized version of the system of equations in which density, taken as the vertical variable, is not varied continuously but in steps: density is restricted to assume a finite number of values. A layered model is the density analog of a *level model*, which is obtained after discretization of the vertical variable z.

Each layer ($k=1$ to m, where m is the number of layers) is characterized by its density ρ_k (unchanging), thickness h_k, Montgomery potential P_k, and horizontal velocity components u_k and v_k. The surface marking the boundary between two adjacent layers is called an *interface* and is described by its elevation z_k, measured (negatively downward) from the mean surface level. The displaced surface level is denoted z_0 (Fig. 12.2a). The interfacial heights can be obtained recursively from the bottom[2]

$$z_m = b, \tag{12.11}$$

upward:

$$z_{k-1} = z_k + h_k, \quad k = m \text{ to } 1. \tag{12.12}$$

This geometrical relation can be regarded as the discretized version of Eq. (12.10) used to define h.

In a similar manner, the discretization of hydrostatic relation (12.5) provides another recursive relation, which can be used to evaluate the Montgomery potential P from the top,

$$P_1 = p_{\text{atm}} + \rho_0 g z_0, \tag{12.13}$$

[2] Note that contrary to our general approach of using indexes which increase with the Cartesian coordinate directions, we choose to increase the index k downward, in agreement with the traditional notation for isopycnal models and with the fact that our new vertical coordinate ρ is increasing downward, too.

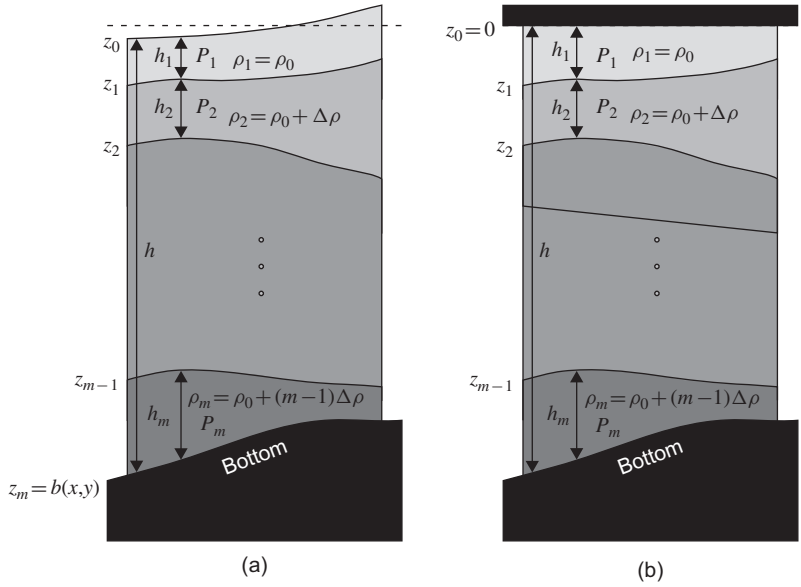

FIGURE 12.2 A layered model with m active layers: (a) with free surface, (b) with rigid lid.

downward:

$$P_{k+1}=P_k+\Delta\rho g z_k, \quad k=1 \text{ to } m-1. \tag{12.14}$$

In writing (12.13), we have selected the uppermost density ρ_1 as the reference density ρ_0. Gradients of the atmospheric pressure p_{atm} rarely play a significant role, and the contribution of p_{atm} to P_1 is usually omitted. If the layered model is for the lower atmosphere, p_{atm} represents a pressure distribution aloft and may, too, be taken as an inactive constant.

When the *reduced gravity*,

$$g'=\frac{\Delta\rho}{\rho_0}g, \tag{12.15}$$

is introduced for convenience, the recursive relations (12.12) and (12.14) lead to simple expressions for the interfacial heights and Montgomery potentials. For up to three layers, these equations are summarized in Table 12.1.

In certain applications, it is helpful to discard surface gravity waves because they travel much faster than internal waves and near-geostrophic disturbances. To do so, we eliminate the flexibility of the surface by imagining that the system is covered by a rigid lid (Fig. 12.2b). This is called the *rigid-lid approximation*, which has already been introduced in the study of barotropic motions in Section 7.5. In such a case, z_0 is set to zero, and there are only $(m-1)$ independent layer thicknesses. In return, one of the Montgomery potentials cannot be

TABLE 12.1 Layered Models

One Layer:	
$z_0 = h_1 + b$	$P_1 = \rho_0 g(h_1 + b)$
$z_1 = b$	
Two Layers:	
$z_0 = h_1 + h_2 + b$	$P_1 = \rho_0 g(h_1 + h_2 + b)$
$z_1 = h_2 + b$	$P_2 = \rho_0 g h_1 + \rho_0 (g + g')(h_2 + b)$
$z_2 = b$	
Three Layers:	
$z_0 = h_1 + h_2 + h_3 + b$	$P_1 = \rho_0 g(h_1 + h_2 + h_3 + b)$
$z_1 = h_2 + h_3 + b$	$P_2 = \rho_0 g h_1 + \rho_0 (g + g')(h_2 + h_3 + b)$
$z_2 = h_3 + b$	$P_3 = \rho_0 g h_1 + \rho_0 (g + g') h_2$
$z_3 = b$	$+ \rho_0 (g + 2g')(h_3 + b)$

TABLE 12.2 Rigid-Lid Models

One Layer:	
$z_1 = -h_1$	P_1 variable
$h_1 = h$, fixed	
Two Layers:	
$z_1 = -h_1$	$P_1 = P_2 + \rho_0 g' h_1$
$z_2 = -h_1 - h_2$	P_2 variable
$h_1 + h_2 = h$, fixed	
Three Layers:	
$z_1 = -h_1$	$P_1 = P_3 + \rho_0 g'(2h_1 + h_2)$
$z_2 = -h_1 - h_2$	$P_2 = P_3 + \rho_0 g'(h_1 + h_2)$
$z_3 = -h_1 - h_2 - h_3$	P_3 variable
$h_1 + h_2 + h_3 = h$, fixed	

derived from the hydrostatic relation. If this potential is chosen as the one in the lowest layer, the recursive relations yield the equations of Table 12.2.

In some other instances, mainly in the investigation of upper-ocean processes, the lowest layer may be imagined to be infinitely deep and at rest (Fig. 12.3). Keeping m as the number of moving layers, we assign to this lowest (abyssal) layer the index $(m+1)$. The absence of motion there implies a uniform Montgomery potential, the value of which may be set to zero without loss of generality: $P_{m+1} = 0$. For up to three active layers, the recursive relations provide equations of Table 12.3. Because these expressions do not involve the full gravity g but only its reduced value g', this type of model is known as a *reduced-gravity model*.

TABLE 12.3 Reduced Gravity Models

One Layer:	
$z_1 = -h_1$	$P_1 = \rho_0 g' h_1$
Two Layers:	
$z_1 = -h_1$	$P_1 = \rho_0 g'(2h_1 + h_2)$
$z_2 = -h_1 - h_2$	$P_2 = \rho_0 g'(h_1 + h_2)$
Three Layers:	
$z_1 = -h_1$	$P_1 = \rho_0 g'(3h_1 + 2h_2 + h_3)$
$z_2 = -h_1 - h_2$	$P_2 = \rho_0 g'(2h_1 + 2h_2 + h_3)$
$z_3 = -h_1 - h_2 - h_3$	$P_3 = \rho_0 g'(h_1 + h_2 + h_3)$

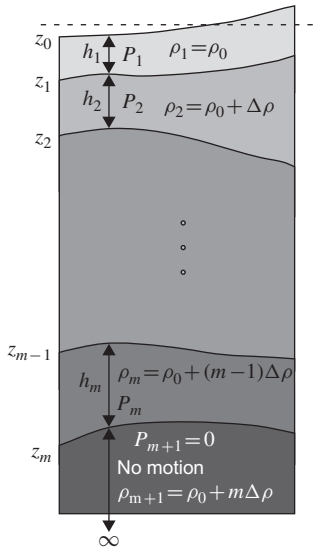

FIGURE 12.3 A reduced-gravity layered model. The assumption of a very deep ocean at rest can be justified by the need to keep the transport hu_{m+1} and kinetic energy hu^2_{m+1} bounded so that velocities must vanish as the depth of the last layer increases to infinity. In this case, the pressure in the deeper layer tends towards a constant, which we may take as zero.

In this table, $z_1 = -h_1$ is an approximation that begs for an explanation. The free surface is not at $z = z_0 = 0$ but given by Eq. (12.13) when we arrive at the surface integrating upward. For a single layer this yields, in the absence of atmospheric pressure variation,

$$P_2 = 0 \rightarrow \quad P_1 = -\Delta\rho g z_1 = \rho_0 g z_0. \tag{12.16}$$

Hence, $gz_0 = -g' z_1$. Since $h_1 = z_0 - z_1$, we get $z_0 = -(g'/g)z_1$ and $h_1 = -(1 + g'/g)z_1 \simeq -z_1$ since $g' \ll g$. This implies a surface lifting over light-water lenses. Indeed, in order to preserve a uniform pressure in the lowest layer, a thickening of the light-water layer must be compensated by an addition of water above mean sea level.

Generalization to more than three moving layers is straightforward. When a configuration with few but physically relevant layers is desired, the preceding derivations may be extended to nonuniform density differences from layer to layer. Mathematically, this would correspond to a discretization of the vertical density coordinate in unevenly spaced gridpoints.

Once the layer thicknesses, interface depths, and layer pressures (more precisely, the Montgomery potentials) are all related, the system of governing equations is completed by gathering the horizontal-momentum equations (12.8a) and (12.8b) and the continuity equation (12.9), each written for every layer.

In Section 11.6, the length $L = NH/\Omega$ was derived as the horizontal scale at which rotation and stratification play equally important roles. It is noteworthy at this point to formulate the analog for a layered system. Introducing H as a typical layer thickness in the system (such as the maximum depth of the uppermost layer at some initial time) and $\Delta\rho$ as a density difference between two adjacent layers (such as the top two), an approximate expression of the stratification frequency squared is

$$N^2 = -\frac{g}{\rho_0}\frac{\mathrm{d}\rho}{\mathrm{d}z} \simeq \frac{g}{\rho_0}\frac{\Delta\rho}{H} = \frac{g'}{H}, \tag{12.17}$$

where $g' = g\ \Delta\rho/\rho_0$ is the reduced gravity defined earlier. Substitution of Eq. (12.17) in the definition of L yields $L \simeq (g'H)^{1/2}/\Omega$. Finally, because the ambient rotation rate Ω enters the dynamics only through the Coriolis parameter f, it is more convenient to introduce the length scale

$$R = \frac{\sqrt{g'H}}{f}, \tag{12.18}$$

called the *radius of deformation*. To distinguish this last scale from its cousin (9.12) derived for free-surface homogeneous rotating fluids (where the full gravitational acceleration g appears), it is customary in situations where ambiguity could arise to use the expressions *internal radius of deformation* and *external radius of deformation* for Eqs. (12.18) and (9.12), respectively. Because density differences within geophysical fluids are typically a percent or less of the average density, the internal radius is most often less than one-tenth the external radius.

When the model consists of a single moving layer above a motionless abyss, the governing equations reduce to

$$\frac{\partial u}{\partial t} + u\frac{\partial u}{\partial x} + v\frac{\partial u}{\partial y} - fv = -g'\frac{\partial h}{\partial x} \tag{12.19a}$$

$$\frac{\partial v}{\partial t} + u\frac{\partial v}{\partial x} + v\frac{\partial v}{\partial y} + fu = -g'\frac{\partial h}{\partial y} \tag{12.19b}$$

$$\frac{\partial h}{\partial t} + \frac{\partial}{\partial x}(hu) + \frac{\partial}{\partial y}(hv) = 0. \tag{12.19c}$$

The subscripts indicating the layer have become superfluous and have been omitted. The coefficient $g' = g(\rho_2 - \rho_1)/\rho_0$ is called the *reduced gravity*. Except for the replacement of the full gravitational acceleration, g, by its reduced fraction, g', this system of equations is identical to that of the shallow-water model over a flat bottom [Eq. (7.17)] and is thus called the *shallow-water reduced-gravity model*. Because the vertical simplicity of this model permits the investigation of a number of horizontal processes with a minimum of mathematical complication, it will be used in some of the following chapters. Finally, recall that the Coriolis parameter, f, may be taken as either a constant (f-plane) or as a function of latitude ($f = f_0 + \beta_0 y$, beta plane).

12.3 POTENTIAL VORTICITY

For layered models, we can reproduce the vorticity analysis that we performed on the shallow-water model (Section 7.4). First, the relative vorticity ζ of the flow at any level is defined as

$$\zeta = \frac{\partial v}{\partial x} - \frac{\partial u}{\partial y}, \tag{12.20}$$

and the expression for potential vorticity is defined in analogy with (7.25):

$$\begin{aligned} q &= \frac{f + \zeta}{h} \\ &= \frac{f + \partial v/\partial x - \partial u/\partial y}{h}, \end{aligned} \tag{12.21}$$

which is identical to the expression for a barotropic fluid, except that the denominator is now a differential thickness given by Eq. (12.10) rather than the full thickness of the system. It can be shown that in the absence of friction, expression (12.21) is conserved by the flow (its material derivative is zero).

The interpretation of this conservation property follows that for a barotropic fluid: When the fluid layer between two consecutive density surface is squeezed (from left to right in Fig. 12.4), conservation of volume demands that it widens, and conservation of circulation in turn requires that it spins less fast; the net effect is that the vorticity $f + \zeta$ decreases in proportion to the thickness h of the fluid layer.

12.4 TWO-LAYER MODELS

For the representation of stratified systems with the simplest possible formalism, the two-layer model is often the tool of choice for it retains the effect of stratification in some basic way through the reduced gravity g' while keeping the number of equations and variables to a minimum. According to Table 12.1,

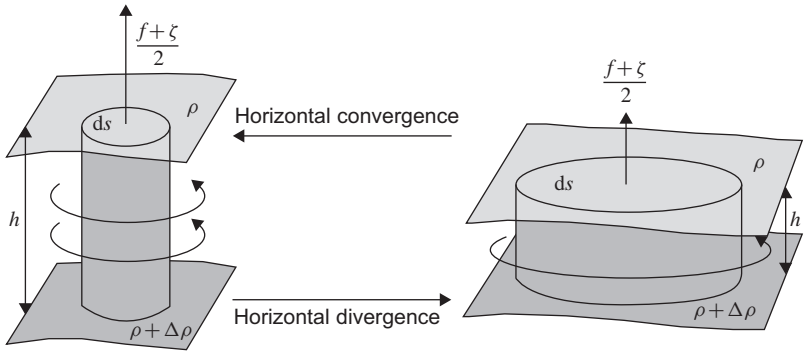

FIGURE 12.4 Conservation of volume and circulation in a fluid undergoing divergence (squeezing) or convergence (stretching). The products of $h\mathrm{d}s$ and $(f+\zeta)\mathrm{d}s$ are conserved during the transformation, implying conservation of $(f+\zeta)/h$, too.

the inviscid governing equations of the two-layer model are

$$\frac{\partial u_1}{\partial t}+u_1\frac{\partial u_1}{\partial x}+v_1\frac{\partial u_1}{\partial y}-fv_1=-g\frac{\partial(h_1+h_2+b)}{\partial x} \tag{12.22a}$$

$$\frac{\partial v_1}{\partial t}+u_1\frac{\partial v_1}{\partial x}+v_1\frac{\partial v_1}{\partial y}+fu_1=-g\frac{\partial(h_1+h_2+b)}{\partial y} \tag{12.22b}$$

$$\frac{\partial u_2}{\partial t}+u_2\frac{\partial u_2}{\partial x}+v_2\frac{\partial u_2}{\partial y}-fv_2=-g\frac{\partial h_1}{\partial x}-(g+g')\frac{\partial(h_2+b)}{\partial x} \tag{12.22c}$$

$$\frac{\partial v_2}{\partial t}+u_2\frac{\partial v_2}{\partial x}+v_2\frac{\partial v_2}{\partial y}+fu_2=-g\frac{\partial h_1}{\partial y}-(g+g')\frac{\partial(h_2+b)}{\partial y} \tag{12.22d}$$

$$\frac{\partial h_1}{\partial t}+\frac{\partial(h_1u_1)}{\partial x}+\frac{\partial(h_1v_1)}{\partial y}=0 \tag{12.22e}$$

$$\frac{\partial h_2}{\partial t}+\frac{\partial(h_2u_2)}{\partial x}+\frac{\partial(h_2v_2)}{\partial y}=0 \tag{12.22f}$$

for the six unknowns h_1, u_1, v_1, h_2, u_2, and v_2.

If we introduce the surface elevation η and the vertical displacement a of the interface between the two layers through $h_1+h_2+b=H+\eta$ and $h_2+b=H_2+a$, where H and H_2 are two constants representing, respectively, the mean surface level and the mean interface level, each measured from the reference datum from which the bottom elevation b, too, is measured (Fig. 12.5), the pressure terms in the x-direction can be rewritten as

$$-g\frac{\partial(h_1+h_2+b)}{\partial x}=-g\frac{\partial\eta}{\partial x} \tag{12.23a}$$

$$-g'\frac{\partial(h_2+b)}{\partial x}=-g'\frac{\partial a}{\partial x} \tag{12.23b}$$

and similarly for the pressure terms in the y-direction.

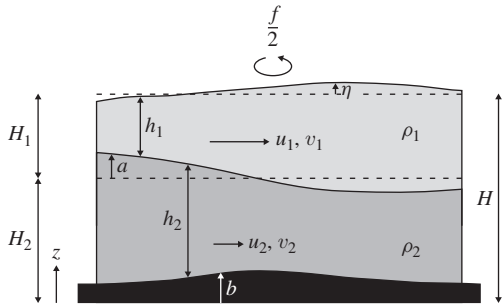

FIGURE 12.5 Notation for the two-layer model with the vertical displacement a of the interface, the sea surface elevation η, and the reference heights H_1 and H_2.

Oftentimes, the two-layer model is used in analytical studies in which case it is also linearized for added simplicity. The equations are then

$$\frac{\partial u_1}{\partial t} - fv_1 = -g\frac{\partial \eta}{\partial x} \tag{12.24a}$$

$$\frac{\partial v_1}{\partial t} + fu_1 = -g\frac{\partial \eta}{\partial y} \tag{12.24b}$$

$$\frac{\partial u_2}{\partial t} - fv_2 = -g\frac{\partial \eta}{\partial x} - g'\frac{\partial a}{\partial x} \tag{12.24c}$$

$$\frac{\partial v_2}{\partial t} + fu_2 = -g\frac{\partial \eta}{\partial y} - g'\frac{\partial a}{\partial y} \tag{12.24d}$$

$$\frac{\partial(\eta - a)}{\partial t} + \frac{\partial(H_1 u_1)}{\partial x} + \frac{\partial(H_1 v_1)}{\partial y} = 0 \tag{12.24e}$$

$$\frac{\partial a}{\partial t} + \frac{\partial[(H_2 - b)u_2]}{\partial x} + \frac{\partial[(H_2 - b)v_2]}{\partial y} = 0, \tag{12.24f}$$

where $H_1 = H - H_2$ is the mean thickness of the top layer.

In the case of flat bottom ($b = 0$), it is interesting to decompose this set of six coupled equations in two sets of three in order to facilitate the solution and clarify the dynamics. For this, we seek proportionality of the type $u_2 = \lambda u_1$, $v_2 = \lambda v_1$ and $\eta = \mu a$ between variables of one layer with those of the other layer. Momentum equations (12.24c)–(12.24d) become identical to (12.24a)–(12.24b) if

$$\frac{\lambda}{1} = \frac{g\mu + g'}{g\mu}, \tag{12.25}$$

while continuity equation (12.24f) replicates (12.24e) if

$$\frac{1}{\mu - 1} = \frac{H_2 \lambda}{H_1}. \tag{12.26}$$

Elimination of μ between the preceding two equations yields an equation for the proportionality coefficient λ:

$$H_2\lambda^2+\left(H_1-H_2-\frac{g'}{g}H_2\right)\lambda-H_1=0. \tag{12.27}$$

Neglecting the small ratio $g'/g=\Delta\rho/\rho_0\ll 1$, the pair of solutions is

$$\lambda=\frac{(H_2-H_1)\pm(H_2+H_1)}{2H_2}. \tag{12.28}$$

Selection of the $+$ sign gives $\lambda=1$, implying a vertically uniform flow ($u_1=u_2$ and $v_1=v_2$). This is called the *barotropic mode*. The interfacial displacement a is related to the surface elevation η by $a=\eta/\mu=H_2\eta/H$ and is thus a vertically prorated fraction of the latter. This mode behaves as if the density difference were absent.

Selection of the $-$ sign in Eq. (12.28) provides the other mode, with $\lambda=-H_1/H_2$, $H_2u_2=-H_1u_1$, and $H_2v_2=-H_1v_1$. The vertically integrated transport is nil for this mode. Equation (12.25) then provides the ratio between vertical elevations, $\mu=-g'H_2/gH$, which is small because it is on the order of the relative density difference $\Delta\rho/\rho_0$. This means that the surface elevation η is weak compared with the interfacial displacement a. For this mode, therefore, the flow is vertically compensated, and its surface is nearly rigid. In other words, it is an internal mode called the *baroclinic mode*.

The equations governing each mode separately can be obtained as follows. For the barotropic mode, we define $u_T=u_1=u_2$, $v_T=v_1=v_2$, and put $a=H_2\eta/H$. Within an error on the order of $\Delta\rho/\rho_0$, the momentum equations reduce to a single pair,

$$\frac{\partial u_T}{\partial t}-fv_T=-g\frac{\partial\eta}{\partial x} \tag{12.29a}$$

$$\frac{\partial v_T}{\partial t}+fu_T=-g\frac{\partial\eta}{\partial y} \tag{12.29b}$$

while each continuity equation reduces to

$$\frac{\partial\eta}{\partial t}+H\frac{\partial u_T}{\partial x}+H\frac{\partial v_T}{\partial y}=0. \tag{12.29c}$$

If we scale time by $1/f$, distances by L and the velocity components by U, the momentum equations tell us that the surface elevation is on the order of fLU/g. Substitution of these scales in the continuity equation then requires that $f(fLU/g)\sim HU/L$, which sets the square of the length scale to $L^2\sim gH/f^2$. This leads us to define the barotropic (or external) radius of deformation:

$$R_{\text{external}}=\frac{\sqrt{gH}}{f}. \tag{12.30}$$

Similarly, the equations governing the baroclinic mode are obtained by defining $u_B = u_1 - u_2$ and $v_B = v_1 - v_2$, and setting $\eta = -(g'H_2/gH)a$. Subtraction of the momentum equations exploiting $H_1 u_1 = -H_2 u_2$ for the baroclinic mode yields

$$\frac{\partial u_B}{\partial t} - f v_B = +g' \frac{\partial a}{\partial x} \tag{12.31a}$$

$$\frac{\partial v_B}{\partial t} + f u_B = +g' \frac{\partial a}{\partial y} \tag{12.31b}$$

while subtraction of the continuity equations gives

$$-\frac{\partial a}{\partial t} + \frac{H_1 H_2}{H}\frac{\partial u_B}{\partial x} + \frac{H_1 H_2}{H}\frac{\partial v_B}{\partial y} = 0. \tag{12.31c}$$

To determine the corresponding radius of deformation, we scale time by $1/f$, distances by L' and the velocity components by U'. According to the momentum equations, the interfacial displacement scales like $fL'U'/g'$. Substitution of these scales in the continuity equation requires $f(fL'U'/g') \sim H_1 H_2 U'/HL'$, which sets the square of the length scale to $L'^2 \sim g' H_1 H_2 / f^2 H$. This in turn leads us to define the baroclinic (or internal) radius of deformation:

$$R_{\text{internal}} = \frac{1}{f}\sqrt{\frac{g' H_1 H_2}{H_1 + H_2}}. \tag{12.32}$$

Note that R_{internal} is significantly shorter than R_{external} because the reduced gravity g' is much smaller than the full gravity g. Another interpretation of the internal radius of deformation is obtained by observing that (12.29) has the same form as (12.31) if η is replaced by $-a$, barotropic velocities by their baroclinic counterpart, g by g', and H by $\bar{h} = H_1 H_2/(H_1 + H_2)$. Hence, the role played by the deformation radius in the barotropic mode is now played by the internal radius for the internal mode. Also, the gravity-wave propagation speed is replaced by the propagation speed of internal gravity waves

$$c = \sqrt{\frac{g' H_1 H_2}{H_1 + H_2}} = \sqrt{g'\bar{h}}, \tag{12.33}$$

which is much lower than the external gravity-wave speed. Because equations (12.31) are structurally identical to (12.29), the solutions will also be, and all wave solutions of the shallow-water equations of Chapter 9 can be applied to the internal mode with the appropriate definitions of gravity and depth. When interpreting the solution we simply have to keep in mind the difference in vertical structure. While the barotropic mode is uniform in the vertical (left panel of Fig. 12.6), the baroclinic mode has zero transport and hence opposite velocities in each layer (right panel of Fig. 12.6).

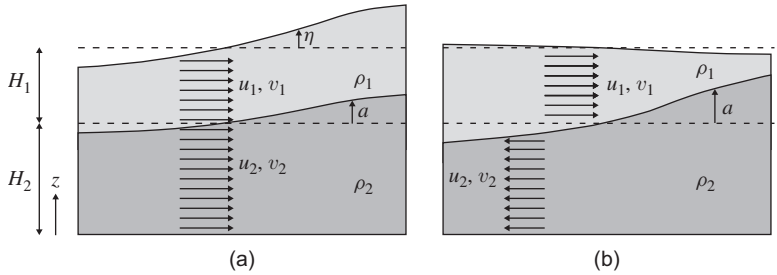

FIGURE 12.6 Barotropic mode (a) and baroclinic mode (b). For the barotropic mode, the interface moves in phase with the sea surface, and velocity is uniform over both layers. In the baroclinic mode, the surface displacement is very weak compared with the interfacial displacement and opposite to it. Velocities in the baroclinic mode are opposite to each other and create no net transport.

When more than two layers are present, the number of modes increases accordingly. For three layers, there will be three modes and so on. In the limit of an infinite number of levels representing continuous stratification, we therefore expect an infinite number of vertical modes, a situation we will encounter again in Section 13.4.

12.5 WIND-INDUCED SEICHES IN LAKES

An interesting application of the two-layer model is to the seiching of thermally stratified lakes. Most lakes of temperate latitudes undergo thermal stratification in summer, and by late summer when surface cooling begins, the water column is often divided into a relatively well mixed and warmer surface layer (called *epilimnion*) and a colder bottom layer (called *hypolimnion*), separated by a thin layer of rapid temperature variation (the *thermocline*). Waves can propagate along both surface and thermocline, and reflection of these waves at the lake's ends can create standing waves called *seiches*. A seiche is usually the response to a wind event: the wind blows for some time, dragging upper-layer water to the downwind side, thereby raising the water level and depressing the thermocline at the downwind end. When the wind relaxes, the situation is out-of-equilibrium, and the warm water begins to slush back and forth across the lake, creating the seiche.

The simplest seiche model assumes no rotational effect (because lakes are typically much smaller than the ocean), a flat bottom and the absence of friction (to simplify the analysis). To illustrate such a seiche model, we take the two-layer model without rotation ($f = 0$) for a domain confined between a flat bottom and two lateral boundaries.

First we concentrate on the barotropic mode with the system of Eqs. (12.29). If we differentiate (12.29a) with respect to x, (12.29b) with respect to y, and (12.29c) with respect to t, and then subtract the first two from the last one,

we obtain

$$\frac{\partial^2 \eta}{\partial t^2} = gH\left(\frac{\partial^2 \eta}{\partial x^2} + \frac{\partial^2 \eta}{\partial y^2}\right), \tag{12.34}$$

We recognize the generic two-dimensional wave equation. Impermeability of lateral boundaries translates into zero normal derivative of η, as seen for example in Eq. (12.29a) when we set $f = 0$ and impose $u = 0$. Thus,

$$\frac{\partial \eta}{\partial x} = 0 \quad \text{at} \quad x = 0, L \tag{12.35}$$

for a basin of length L in the x-direction. Similarly in the y-direction,

$$\frac{\partial \eta}{\partial y} = 0 \quad \text{at} \quad y = 0, W \tag{12.36}$$

if the width is W.

For such a rectangular domain, it is easily verified that

$$\eta = A\cos(\omega t)\cos\left(\frac{m\pi x}{L}\right)\cos\left(\frac{n\pi y}{W}\right) \tag{12.37}$$

is the solution of Eq. (12.34) satisfing all four boundary conditions as long as m and n are integers and provided that

$$\omega^2 = gH\left(\frac{m^2\pi^2}{L^2} + \frac{n^2\pi^2}{W^2}\right) \tag{12.38}$$

The solution $m = n = 0$ corresponds to a situation of rest, and, for an elongated basin with $L \geq W$, the gravest mode is obtained for $m = 1$, $n = 0$. In this case, the seiche is a standing wave of frequency

$$\omega = \pi\frac{\sqrt{gH}}{L}. \tag{12.39}$$

The gravest mode is of special importance because it is the one with the smoothest structure and thus the one that is dissipated at the slowest rate. Also, wind forcing is more likely to generate the gravest mode because atmospheric forcing generally varies weakly over the length of a lake and can, at a first approximation, be considered uniform.

We can immediately extend the previous result to the baroclinic mode by replacing gH by $g'H_1H_2/(H_1 + H_2)$ and interpret the velocity oscillations in the light of the baroclinic mode of Fig. 12.6. The lowest-mode frequency becomes

$$\omega = \frac{\pi}{L}\sqrt{g'\frac{H_1H_2}{H_1 + H_2}} \tag{12.40}$$

and corresponds to a much longer period of oscillation. Sloshing of the density interface is similar to an oscillation of the surface. In an internal seiche,

however, the upper-layer velocity is opposite to that in the lower layer, so that water going to one side of the lake near the surface is compensated by flow near the bottom to the other side of the lake, with no appreciable change in surface elevation.

When rotation comes into play (f no longer zero), the standing wave pattern is no longer formed by the superposition of pure gravity waves but by the superposition of inertial-gravity waves, and the mathematical solution is more complicated. In particular, so-called *amphidromic points*, at which the amplitude is nil, can arise (see Section 9.8). The interested reader is referred to Taylor (1921).

Seiches occur not only in lakes but also in the coastal ocean. In the Adriatic Sea, a longitudinal seiche following an episode of sirocco wind can combine with a tidal elevation to create flooding in Venice (Cushman-Roisin, Gačić, Poulain & Artegiani, 2001). Internal seiches have also been observed in Scandinavian fjords (e.g., Arneborg & Liljebladh, 2001).

12.6 ENERGY CONSERVATION

Inspection of energetics in a layered model is insightful because it provides the formulation of the quantities that serve as kinetic and potential energies. To do this, we reinstate the nonlinear terms, the Coriolis acceleration and uneven bottom topography but restrict our attention to the two-layer system described by Eq. (12.22) with the pressure gradients given by Eq. (12.23).

In the absence of friction, no dissipation is present, and we expect conservation of total energy, sum of kinetic energy (KE), and potential energy (PE). These are defined respectively as:

$$\begin{aligned} KE &= \frac{\rho_0}{2}\iiint \left(u^2+v^2\right)\mathrm{d}z\,\mathrm{d}y\,\mathrm{d}x \\ &= \frac{\rho_0}{2}\iint\left[\int_b^{H_2+a}\left(u_2^2+v_2^2\right)\mathrm{d}z+\int_{H_2+a}^{H_1+H_2+\eta}\left(u_1^2+v_1^2\right)\mathrm{d}z\right]\mathrm{d}y\,\mathrm{d}x \\ &= \frac{\rho_0}{2}\iint\left[h_2\left(u_2^2+v_2^2\right)+h_1\left(u_1^2+v_1^2\right)\right]\mathrm{d}y\,\mathrm{d}x. \end{aligned} \tag{12.41}$$

$$\begin{aligned} PE &= \iiint \rho g z\,\mathrm{d}z\,\mathrm{d}y\,\mathrm{d}x \\ &= \iint\int_b^{H_2+a}\rho_2 g z\,\mathrm{d}z\,\mathrm{d}y\,\mathrm{d}x+\iint\int_{H_2+a}^{H_1+H2+\eta}\rho_1 g z\,\mathrm{d}z\,\mathrm{d}y\,\mathrm{d}x \end{aligned} \tag{12.42}$$

Note how we used the Boussinesq approximation: The actual density (ρ_1 or ρ_2) is used next to g in the potential energy but is replaced by the reference density (ρ_0) in the kinetic energy.

Mass conservation in a closed basin leads obviously to

$$\iint \eta \,\mathrm{d}y\,\mathrm{d}x = 0 \qquad \iint a \,\mathrm{d}y\,\mathrm{d}x = 0 \tag{12.43}$$

so that, up to an additive constant, potential energy can be expressed as

$$PE = \frac{\rho_0}{2} \iint \left(g\eta^2 + g' a^2 \right) \mathrm{d}y\,\mathrm{d}x, \tag{12.44}$$

which shows that vertical displacements a of the interface need to be much larger than surface elevations η to contribute equally to potential energy. With the previous definition, the reference state $\eta = 0$ and $a = 0$ has zero potential energy. Any departure from this situation leads to a positive amount of potential energy. This amount is thus called available potential energy (see also Section 16.4).

To construct the energy budget, we multiply (12.22a) by $h_1 u_1$ and exploit (12.22e) to obtain first:

$$\begin{aligned} &\frac{\partial}{\partial t}\left(\frac{h_1 u_1^2}{2}\right) + \frac{\partial}{\partial x}\left(u_1 \frac{h_1 u_1^2}{2}\right) + \frac{\partial}{\partial y}\left(v_1 \frac{h_1 u_1^2}{2}\right) \\ &\quad - f h_1 u_1 v_1 h_1 = -\frac{\partial (g h_1 u_1 \eta)}{\partial x} + g\eta \frac{\partial (h_1 u_1)}{\partial x}. \end{aligned} \tag{12.45}$$

We then multiply (12.22b) by $h_1 v_1$, exploit (12.22e), add the result to Eq. (12.45), and integrate over a closed or periodic domain to obtain

$$\frac{\mathrm{d}}{\mathrm{d}t} \iint \left(h_1 \frac{u_1^2 + v_1^2}{2} \right) \mathrm{d}y\,\mathrm{d}x = \iint g\eta \left[\frac{\partial (h_1 u_1)}{\partial x} + \frac{\partial (h_1 v_1)}{\partial y} \right] \mathrm{d}y\,\mathrm{d}x, \tag{12.46}$$

which shows that the amount of upper-layer kinetic energy can be altered by the divergence of the transport.

Similarly, we can obtain the equation governing the evolution of kinetic energy in the second layer:

$$\frac{\mathrm{d}}{\mathrm{d}t} \iint \left(h_2 \frac{u_2^2 + v_2^2}{2} \right) \mathrm{d}y\,\mathrm{d}x = \iint \left(g\eta + g' a \right) \left[\frac{\partial (h_2 u_2)}{\partial x} + \frac{\partial (h_2 v_2)}{\partial y} \right] \mathrm{d}y\,\mathrm{d}x. \tag{12.47}$$

For the potential-energy budget, we multiply (12.22e) by $g\eta$ and integrate over the domain:

$$\frac{\mathrm{d}}{\mathrm{d}t} \iint g \frac{\eta^2}{2} \mathrm{d}y\,\mathrm{d}x = \iint \left\{ g\eta \frac{\partial a}{\partial t} - g\eta \left[\frac{\partial (h_1 u_1)}{\partial x} + \frac{\partial (h_1 v_1)}{\partial y} \right] \right\} \mathrm{d}y\,\mathrm{d}x. \tag{12.48}$$

We then multiply (12.22f) by $g'a$, exploit the relation $\partial h_2/\partial t = \partial a/\partial t$, and integrate over the domain yields, to obtain

$$\frac{\mathrm{d}}{\mathrm{d}t}\iint g'\frac{a^2}{2}\mathrm{d}y\,\mathrm{d}x = \iint -g'a\left[\frac{\partial(h_2u_2)}{\partial x}+\frac{\partial(h_2v_2)}{\partial y}\right]\mathrm{d}y\,\mathrm{d}x. \tag{12.49}$$

Using Eq. (12.22f) to replace $\partial a/\partial t$ in the right-hand side of Eq. (12.48), we can identify similar terms on the right-hand side of Eqs. (12.46)–(12.49) but with opposite signs. These terms represent energy exchange between the different forms of potential and kinetic energy. Hence, by adding the four equations, these terms cancel one another out. After multiplying by ρ_0, we ultimately obtain the statement of energy conservation:

$$\frac{\mathrm{d}}{\mathrm{d}t}(PE+KE)=0. \tag{12.50}$$

Besides certifying the expressions for kinetic and potential energy, this analysis has also identified for us the expressions for the exchange terms between the different forms of energy. The underlying mechanism is convergence/divergence of the horizontal flow (affecting kinetic energy) accompanied by piling/dropping of water (affecting potential energy in a compensating way).

12.7 NUMERICAL LAYERED MODELS

The development of numerical models based on the governing equations written in isopycnal coordinates is simplified by the fact that a discretization of the vertical coordinate is already performed through the layering (Section 12.2). Indeed, we arrived at governing equations for a set of m layers, in which the vertical coordinate no longer appears. In other words, we replaced a three-dimensional problem by m coupled two-dimensional problems.

Since it is straightforward to generalize the layering approach and use different values of $\Delta\rho$ across layers, we can easily define layers so as to follow physically meaningful water masses. Once the $\Delta\rho$ values are assigned to define the layers, the only discretization that remains to be done is the one related to the two-dimensional "horizontal" structure, a task we already performed in the context of the shallow-water equations (Section 9.7 and 9.8). Since the governing equations of each isopycnal layer are very similar to those of the inviscid shallow-water equations, all we have to do is to "repeat" the implementation of the shallow-water equations for each layer and adapt the pressure force. Here, we can notice how easily pressure can be calculated in the layered system once the layer thicknesses are known by simply integrating (12.14), or its straightforward generalization when density differences vary between layers. To calculate layer thicknesses, the volume-conservation equations are at our disposal and are also similar to those of the shallow-water system. Finally, as for shallow-water equations, additional processes neglected up to now can be reinstated. Bottom and top stresses can be taken into account at the lowest and uppermost layers

by adding a frictional term as we did for the shallow-water equations. Also friction between layers can be accommodated by introducing terms that depend on the velocity difference across each interface. These internal friction terms must appear with opposite signs in the equations for the two layers scrubbing against each other, so that the momentum lost by one is gained by the other.

Finally, unresolved horizontal subgrid scale processes can be parameterized, for example using a lateral eddy viscosity (i.e., adding a Laplacian term). It is noteworthy to point out here that lateral diffusion formulated in the new coordinate system (with $\partial/\partial x$ derivatives taken at constant ρ) corresponds to mixing along isopycnals rather than in the horizontal plane (constant z) (see Section 20.6.2). This is generally considered advantageous if we consider that shorter-scale movements are more easily generated along a density surface because they do not implicate any buoyancy force. The parameterization of subgrid scale processes as diffusion along isopycnal surfaces is called *isopycnal diffusion* and is naturally included in the governing equations of layered models. In other words, no diapycnal (i.e., across-density) diffusion and erosion of stratification will take place, and water masses are conserved.

This is at the same time a major strength and weakness of the layer formulation. It is an advantage if the physical system prevents mixing, and the model simulates motions and oscillations without any numerical destruction of the density stratification, otherwise a common issue affecting three-dimensional models. However, if vertical mixing or vertical convection is significant in the physical system, the layered model requires an additional term to represent transfer (entrainment) of fluid from one layer into another. The danger is then that a layer may lose so much of its fluid and become so thin that is becomes dynamically irrelevant and should be removed, at least in some region of the domain. In addition, layer interfaces can intersect the bottom or top (Fig. 12.7). In other words, the region where each layer exists may not be the entire domain and may furthermore change over time. Tracking the edges of the layers is a problem that is far from trivial.

The problem is even worse when gravitational instabilities are present because the coordinate transformation then loses its validity. Problems associated with strong vertical mixing and gravitational instabilities explain why isopycnal models are rarely used for atmospheric simulations, where convection and associated gravitational instabilities are much more frequent than in the ocean.

Another difficulty with oceanic layered models is the fact that by construction, density is constant within each layer so that temperature and salinity cannot vary independently. Yet, physical boundary conditions are independent for temperature (heat flux) and salinity (evaporation, precipitation). Finally, isopycnal models are not easily applied when the same domain includes both the deep ocean and coastal areas because the variety of density structure does not lend itself to be represented with a single set of density layers.

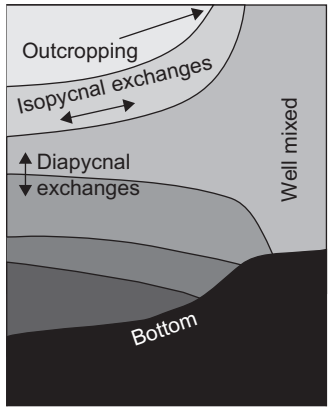

FIGURE 12.7 The application of a layered model needs some special care when isopycnals intersect the surface (outcropping), the bottom, or one another. Surface outcropping typically arises in the vicinity of fronts or following strong mixing events, while bottom intersection is likely to occur in regions of steep topography.

Numerical layered models offer a choice between the original model, the rigid-lid approximation, and the reduced-gravity version. This choice affects the numerical properties. For example, the reduced-gravity model has gravity g replaced by g' in all its equations, and as a result no longer allows propagation of surface gravity waves. This can be desirable from a numerical perspective. Indeed, numerical stability requirements of shallow-water models are typically of the type

$$\frac{\sqrt{gh}\Delta t}{\Delta x} \leq \mathcal{O}(1), \tag{12.51}$$

(see Section 9.7). With gravity replaced by reduced gravity, the numerical stability constraint becomes

$$\frac{\sqrt{g'h}\Delta t}{\Delta x} \leq \mathcal{O}(1), \tag{12.52}$$

which is much less stringent than (12.51) because $g' \ll g$. The full gravity g also disappears from the models using the rigid-lid approximation, and no stability condition of the type (12.51) applies. Longer time steps may be used in either case.

For the original version of the layered model, using neither rigid-lid approximation nor the reduced-gravity approach, surface gravity waves are possible, and stability condition (12.51) can be very constraining compared with other numerical stability conditions. Some optimization becomes necessary. A brute force approach would be implicit treatment of the terms responsible for the stability constraint. The velocity field in the equation governing layer thickness should then be treated implicitly together with the surface height term in the momentum equations. The latter appears in all momentum equations because the surface pressure is $P_1 = p_{\text{atm}} + \rho_0 g\eta$ according to Eq. (12.13), and the sum

(12.14) means that η becomes part of the pressure terms in all other layers. With an implicit scheme, this means that all equations must be solved simultaneously, forming a rather large, though sparse, linear system to be inverted at every time step. Using a long time step for the propagation of the fast waves also degrades the propagation properties of these waves.

A better approach is to recall that surface gravity waves are generated by surface displacements accompanied by divergence–convergence of the vertically integrated flow and to treat the corresponding subset of the dynamics with a shorter time step than the rest. This can be accomplished by averaging over the vertical in order to construct an equation governing the barotropic component of the flow. The nonlinear terms, however, cause a difficulty because the average of products is not equal to the product of the averages. The result is an equation governing the barotropic mode that contains some baroclinic terms. Fortunately, since those vary slowly whereas the barotropic mode evolves rapidly, they may be held frozen while marching the rest of the equation forward. This is called *mode splitting* (Fig. 12.8).

In such scheme, the surface elevation η is marched N times, whereas the rest of the dynamics is marched forward only once. In view of the typical values of g and g', the longer time step is typically an order of magnitude larger than the short time step required for surface waves, and since the solution of the shallow-water equations with the short time step involves only three instead of $3m$ equations, an order of magnitude can be gained in computational cost by the mode-splitting technique.

At the end of the N barotropic steps and the subsequent single baroclinic step, a problem may occur. The momentum equations of each layer calculated with the new elevation η^{n+1} from the barotropic equation will lead to

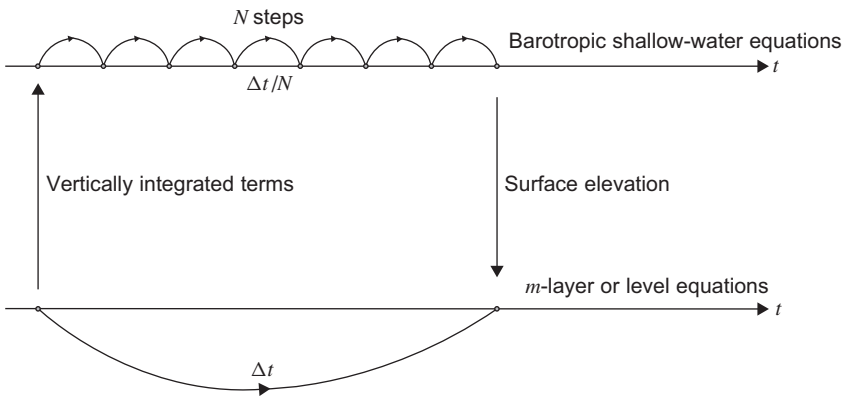

FIGURE 12.8 At a given time step, information from all layer thicknesses permit the calculation of the slow baroclinic terms, which can be held temporarily frozen. The barotropic component of the flow (shallow-water type equation) can then be marched forward in time over several short time steps, until the overall, longer time step Δt is covered. Then, the surface height η at the new time level can be used in all layers to forward in time the internal structure of the flow.

velocities at the new time level u_k^{n+1}, v_k^{n+1}. The transport obtained by summing up these velocities weighted by the corresponding layer thicknesses will, however, be different from the transport that would have been obtained after N substeps because of nonlinearities in the equations. If nothing is done to correct this mismatch, instabilities can occur (e.g., Killworth, Stainforth, Webb & Paterson, 1991). The problem can be avoided by correcting the velocity fields obtained after solving the individual layer equations so as to make sure that their weighted sum equals the predicted transport from the shallow-water equations. This approach can also be applied to level models or any 3D model with a free surface. The general idea remains the preliminary vertical integration of the governing equations in order to make the barotropic component explicit and to march forward in time the latter with a shorter time step than the rest of the equations.

Aside from the aforementioned difficulties, we can retain the distinct advantage of aligning coordinate lines (and hence numerical grids) with dynamically significant features. This explains the success of numerical layer models, and several widely used numerical isopycnal models are based on the successive developments of Hurlburt and Thompson (1980), Bleck, Rooth, Hu and Smith (1992), and Hallberg (1995). The modern tendency, however, is to go beyond pure layer models in favor of more general vertical-coordinate models, which we will encounter in Section 20.6.1.

12.8 LAGRANGIAN APPROACH

In a layered model, the conservation equation for ρ is vastly simplified because coordinate surfaces coincide with material surfaces of the flow. This is the hallmark of a Lagrangian approach. As opposed to a Eulerian representation of the flow, in which flow characteristics are assigned to fixed points, in a Lagrangian approach, characteristics of the flow are tracked following fluid parcels. A layered model, however, does this only in the vertical direction, not in all three directions of space. This motivates us nonetheless to explore here what fully Lagrangian models can offer.

A fully Lagrangian model tracks not merely material surfaces but individual fluid parcels, and just as the choice of density as the vertical coordinate in a layered model eliminates the vertical velocity from advection, a fully Lagrangian approach eliminates all advection terms and is therefore most interesting in problems associated with the discretization of advection terms. In Section 6.4, the astute reader may have already wondered why we went through all these complicated Eulerian schemes to find the solution to a pure-advection problem, which is stated so simply in terms of the material derivative

$$\frac{\mathrm{d}c}{\mathrm{d}t} = 0 \tag{12.53}$$

and has such a disarming solution $c = c^0$ for a parcel with initial value c^0. A single fluid parcel, however, does not provide the concentration everywhere across

the domain but only at its particular location. To determine the concentration distribution, we first need to calculate the trajectories of an ensemble of parcels launched at different locations. For this, we need to return to the basic definition of velocity:

$$\frac{\mathrm{d}x}{\mathrm{d}t} = u[x(t), y(t), z(t), t] \tag{12.54a}$$

$$\frac{\mathrm{d}y}{\mathrm{d}t} = v[x(t), y(t), z(t), t] \tag{12.54b}$$

$$\frac{\mathrm{d}z}{\mathrm{d}t} = w[x(t), y(t), z(t), t], \tag{12.54c}$$

and integrate over time for each of, say, N fluid parcels. If the starting locations are (x_p^0, y_p^0, z_p^0) for $p = 1$ to N, integration of the previous equations provides the positions $[x_p(t), y_p(t), z_p(t)]$ of the same N parcels at time t. This is the core of a *Lagrangian approach*, and it obviously requires the knowledge of the velocity field at all times.

The value of c at any point in the domain can then be obtained by interpolation from the closest parcels or by averaging within grid cells (*binning*), depending on the number of parcels in the region. In either approach, for the method to work, the domain must at any moment be as uniformly covered as possible by a sufficiently dense number of parcels. If there are regions nearly void of parcels, concentrations cannot be inferred there, and this is the first problem with the Lagrangian approach: For an initially relatively uniform distribution of parcels, convergence and divergence of the flow can sooner or later concentrate parcels in some regions and depopulate other parts of the domain (Fig. 12.9). Algorithms must be designed to eliminate parcels in regions where they are redundant and to add new parcels in empty regions. Roughly, if L and H are, respectively, the horizontal and vertical length scales of the 3D flow with surface $\mathcal{S}$ and depth D, we need at least $D\mathcal{S}/(L^2H)$ parcels, which is about the required number of grid boxes, (1.17), needed in an Eulerian model of the same flow. However, because the Lagrangian parcels have a tendency to cluster and leave regions with lower coverage, 10–100 times more parcels are typically needed to resolve the same flow.

The time integration itself also imposes some constraints on the method: For accurate time integration of Eq. (12.54), we must be able to respect the spatial variations of the velocity field during a time step, and this requires

$$U\Delta t \leq L, \tag{12.55}$$

or the trajectory calculation will be inaccurate. For the same reason, we must also respect the time variations of the flow, $\Delta t \ll T$ if the flow varies with time scale T.

Another important aspect is related to the integration of the trajectories. In addition to the aforementioned accuracy requirement, two sources of errors

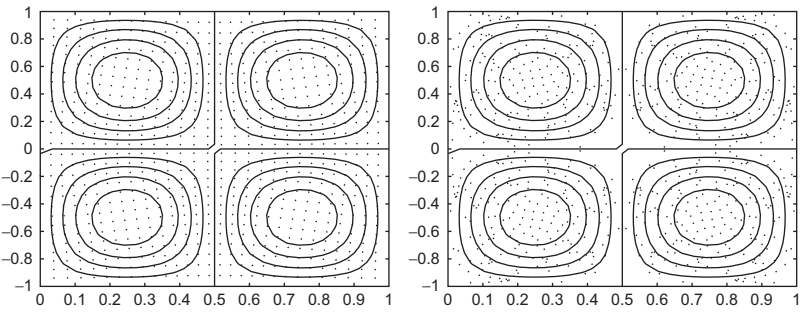

FIGURE 12.9 Calculation of particle displacement in a flow field with multiple circulation cells. Fluid parcels follow the stationary streamfunction (solid line) and deplete some regions. Use `traj2D.m` to view an animated version.

are encountered. First, the time discretization itself does not generally ensure a reversible calculation. If time or velocities are reversed, the numerical integration does not return parcels to their initial positions (see Numerical Exercise 12.5). Therefore, the time integration produces some dispersion. The second source of error is related to the knowledge of the velocity field itself calculated by a model and thus available only at discrete locations. For a velocity field given on a rectangular grid, calculations of a trajectory passing through the arbitrary location $[x(t), y(t), z(t)]$ require interpolation among adjacent grid points. The resulting interpolation error will then affect the subsequent calculation of the trajectory and induce some additional dispersion among parcels.

Except for those restrictions, the Lagrangian approach is easily implemented. Diffusion can be taken into account by simulating mixing through random displacement of particles, also called *random walk*, according to

$$x^{n+1} = x^n + \int_{t^n}^{t^{n+1}} \left[u(x(t), y(t), z(t), t) + \frac{\partial \mathcal{A}}{\partial x} \right] \mathrm{d}t + \sqrt{2\Delta t \mathcal{A}}\, \xi \tag{12.56}$$

where $\mathcal{A}$ is the desired diffusivity, and ξ is a random variable of Gaussian[3] distribution with zero mean and unit standard deviation (e.g., Gardiner, 1997).

It can be shown (e.g., Gardiner, 1997; Spagnol et al., 2002; Spivakovskaya, Heemink & Deleersnijder, 2007) that the previous stochastic equation leads to

[3] It should be noted that in most models the random variable does not obey a Gaussian but a uniform distribution. This is acceptable as long as time steps are short so that performing a succession of many time steps amounts to adding up a large number of random steps, and, by virtue of the *central limit theorem* (e.g., Riley, Hobson & Bence, 1977), the many-step process follows the Gaussian distribution.

particle distributions consistent with

$$\frac{\partial c}{\partial t}+u\frac{\partial c}{\partial x}=\frac{\partial}{\partial x}\left(\mathcal{A}\frac{\partial c}{\partial x}\right). \tag{12.57}$$

A large number of fluid parcels moved according to Eq. (12.56) then mimic the concentration evolution of Eq. (12.57). The role of the term $\partial\mathcal{A}/\partial x$ in the time integral can be easily understood and illustrated in a situation of a local minimum of $\mathcal{A}$ within the domain of interest, such as near a pycnocline (Numerical Exercise 12.8).

If momentum equations, too, are solved by a Lagrangian approach, the momentum of a particle is changed along its trajectory, mostly by the pressure-gradient force. An elegant method among others to obtain the pressure distribution corresponding to a given set of mass-endowed particles is the particle-in-cell method (Cushman-Roisin, Esenkov & Mathias, 2000; Esenkov & Cushman-Roisin, 1999; Pavia & Cushman-Roisin, 1988).

ANALYTICAL PROBLEMS

12.1. Generalize the theory of the coastal Kelvin wave (Section 9.2) to the two-layer system over a flat bottom and under a rigid lid. In particular, what are the wave speed and trapping scale?

12.2. In the case of the shallow-water reduced-gravity model, derive an energy-conservation principle. Then, separate the kinetic and potential energy contributions.

12.3. Show that a steady flow of the shallow-water reduced-gravity system conserves the Bernoulli function $B=g'h+(u^2+v^2)/2$.

12.4. Establish the equations governing motions in a one-layer model above an uneven bottom and below a thick, motionless layer of slightly lesser density.

12.5. Seek a solution to the shallow-water reduced-gravity model of the type

$$h(x,t)=x^2A(t)+2xB(t)+C(t) \tag{12.58a}$$
$$u(x,t)=xU_1(t)+U_0(t) \tag{12.58b}$$
$$v(x,t)=xV_1(t)+V_0(t). \tag{12.58c}$$

To what type of motion does this solution correspond? What can you say of its temporal variability? (Take $f=$ constant.)

12.6. Using the rigid-lid approximation in the shallow-water equations (i.e., a single density layer), analyze the dispersion relation of waves on the beta plane. Show that there are no gravity waves and that the only dispersion relation that remains corresponds to planetary waves (9.27). How can the

difference in dispersion relation be interpreted in terms of the hypotheses used in the rigid-lid approximation? (*Hint*: Look again at Section 7.5.)

12.7. In the western Mediterranean Sea, Atlantic waters flow along theAlgerian coast and are slightly lighter than the Mediterranean water. If the density difference is 1.0 kg/m^3, and the thickness of the Atlantic water layer is 150 m, how large is the sea surface displacement associated with the intrusion of the lighter water? (*Hint*: Assume the lower layer to be at rest.)

12.8. Prove the assertion made below Eq. (12.21) that the potential vorticity so defined is indeed conserved along the flow in the absence of friction. Specifically, show that its material derivative, using Eq. (12.7), vanishes.

NUMERICAL EXERCISES

12.1. Adapt the shallow-water equation model developed in Numerical Exercise 9.3 to simulate seiches in a lake with a reduced-gravity model.

12.2. Discretize the linearized two-layer model in time and with a horizontal Arakawa grid of your choice. Use a discretization that does not require the solution of a linear system. Provide a stability analysis neglecting the Coriolis force.

12.3. Implement the discretization of Numerical Exercise 12.2 and reproduce numerically the solution of Section 12.5.

12.4. Explore the implicit treatment of surface elevation in the barotropic component of the layer equations. Use an Arakawa C-grid and implicit treatment of both the divergence term in volume conservation and pressure gradient in the momentum equations. Neglect the Coriolis force. Eliminate the yet unknown velocity components from the equations to arrive at an equation for η^{n+1}. Compare the approach with the pressure calculation used in conjunction with the rigid-lid approximation of Section 7.6 and interpret what happens when you take very long time steps.

12.5. Use different time-integration techniques to calculate trajectories associated with the following 2D current field:

$$u = -\cos(\pi t)\, y, \qquad v = +\cos(\pi t)\, x \tag{12.59}$$

from $t = 0$ to $t = 1$ and interpret the results. Prove that the trapezoidal scheme is reversible in time.

12.6. Implement a random walk into the calculation of the trajectories of Numerical Exercise 12.5 and verify the dispersive nature of the random walk. (*Hint*: Start with a dense cloud of particles in the middle of the domain.)

12.7. Use a large number of particles to advect the tracer field of Fig. 6.18 by distributing them initially on a regular grid. Look at `tvdadv2D.m` to see how the velocity field and initial concentration distribution are defined. Which problem do you face when you need to calculate the concentration at an arbitrary position at a later moment?

12.8. Implement Eq. (12.56) without advection in a periodic domain between $x = -10L$ and $x = 10L$ and with diffusion given by

$$\mathcal{A} = \mathcal{A}_0 \tanh^2\left(\frac{x}{L}\right). \tag{12.60}$$

Start with a uniform distribution of particles in the left half of the domain ($x < 0$) and no particles in the other half ($x > 0$). Simulate the evolution with and without the term $\partial\mathcal{A}/\partial x$ and discuss your findings. Take $L =$ 1000 km and $\mathcal{A}_0 = 1000\,\mathrm{m}^2/\mathrm{s}$. (*Hint*: Periodicity of the domain can be ensured by proper repositioning of particles when they cross a boundary. Modulo is an interesting and useful function here.)

Raymond Braislin Montgomery
1910–1988

A student of Carl-Gustav Rossby, Raymond Braislin Montgomery earned a reputation as a brilliant descriptive physical oceanographer. Applying dynamic results derived by his mentor and other contemporary theoreticians to observations, he developed precise means of characterizing water masses and currents. By his choice of analyzing observations along density surfaces rather than along level surfaces, an approach that led him to formulate the potential now bearing his name, Montgomery was able to trace the flow of water masses across ocean basins and to arrive at a lucid picture of the general oceanic circulation. Montgomery's lectures and published works, marked by an unusual attention to clarity and accuracy, earned him great respect as a critic and reviewer. (*Photo by Hideo Akamatsu — courtesy of Mrs. R. B. Montgomery*)

James Joseph O'Brien
1935–

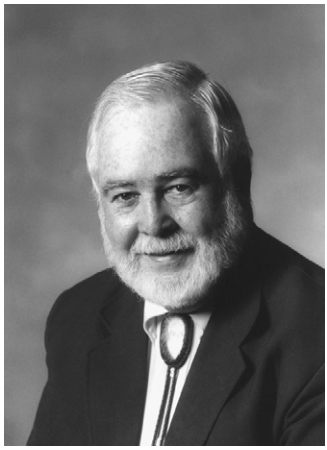

After a professional start as a chemist, Jim O'Brien decided to change career and turned to oceanography, a discipline in which he found greater intellectual challenges. This was around 1970, when computers were beginning to reveal their power for solving complicated dynamical systems, such as the ocean circulation. O'Brien quickly rose to become a leader in numerical modeling of physical oceanography and air–sea interactions. His early models of coastal upwelling taught us much about this important oceanic process. He was the first to show by numerical simulation that knowledge of wind over the tropical Pacific Ocean is essential to represent El Niño events. In the course of his numerical applications (many of them using layered models), he also discovered that the error made on the group velocity in a computer model is often more troublesome than the error made on the phase propagation speed.

Professor O'Brien has communicated his boundless enthusiasm for numerical modeling, oceanography, and air-sea interactions to a large number of graduate students and young researchers, who went on to occupy prominent positions across the United States and the world. (*Photo credit: Florida State University*)